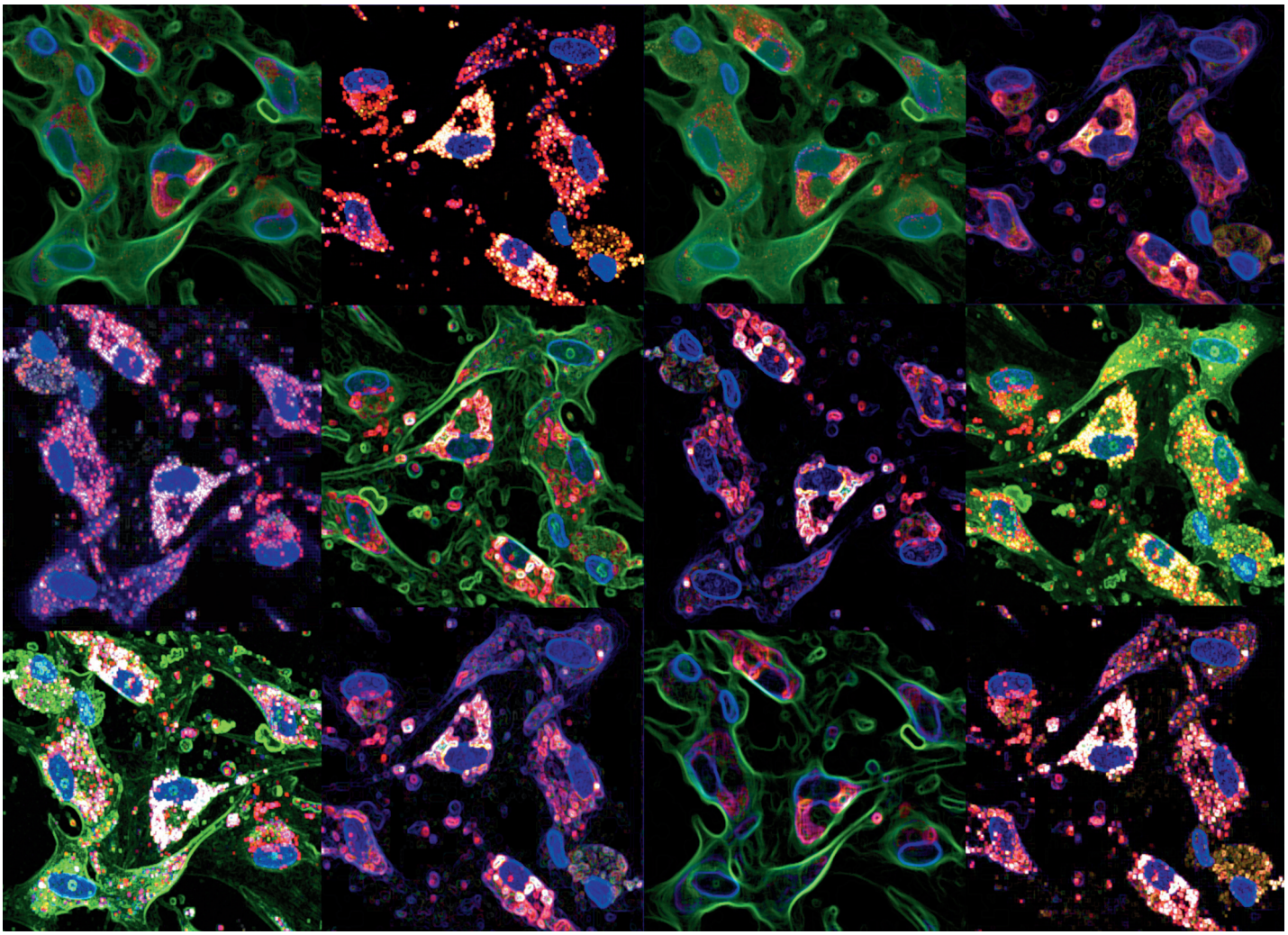

Showcasing research from the Langer Lab, Massachusetts Institute of Technology, Cambridge, USA and the Aikawa-Aikawa Group, Harvard University, Boston, USA.

Controlled delivery of gold nanoparticle-coupled miRNA therapeutics *via* an injectable self-healing hydrogel

Engineered gold nanoparticles functionalized with RNA therapeutics were loaded into a shear thinning, self-healing hydrogel. The injectable hydrogel provided controlled release of the nanoparticles, which successfully infiltrated valvular interstitial cells in a 3D bioprinted heart valve disease model. The RNA therapeutics remained active and suppressed their targets in HEK293 cells *in vitro*. Furthermore, *in vivo* experiments demonstrated renal clearance 11 days after subcutaneous injection, highlighting the potential for translation of this drug delivery platform technology.

As featured in:

See Elena Aikawa, Robert S. Langer *et al.*, *Nanoscale*, 2021, **13**, 20451.

ROYAL SOCIETY OF CHEMISTRY

rsc.li/nanoscale

Registered charity number: 207890

Nanoscale

PAPER

View Article Online
View Journal | View Issue

Cite this: *Nanoscale*, 2021, **13**, 20451

Controlled delivery of gold nanoparticle-coupled miRNA therapeutics *via* an injectable self-healing hydrogel†

Casper F. T. van der Ven, [a,b,c,d] Mark W. Tibbitt, [d,e] João Conde, [f,g] Alain van Mil, [a,b,h] Jesper Hjortnaes, [a,b] Pieter A. Doevendans, [b,h] Joost P. G. Sluijter, [a,b] Elena Aikawa *‡[c,i] and Robert S. Langer*‡[d,j]

Differential expression of microRNAs (miRNAs) plays a role in many diseases, including cancer and cardiovascular diseases. Potentially, miRNAs could be targeted with miRNA-therapeutics. Sustained delivery of these therapeutics remains challenging. This study couples miR-mimics to PEG-peptide gold nanoparticles (AuNP) and loads these AuNP-miRNAs in an injectable, shear thinning, self-assembling polymer nanoparticle (PNP) hydrogel drug delivery platform to improve delivery. Spherical AuNPs coated with fluorescently labelled miR-214 are loaded into an HPMC-PEG-b-PLA PNP hydrogel. Release of AuNP/miRNAs is quantified, AuNP-miR-214 functionality is shown *in vitro* in HEK293 cells, and AuNP-miRNAs are tracked in a 3D bioprinted human model of calcific aortic valve disease (CAVD). Lastly, biodistribution of PNP-AuNP-miR-67 is assessed after subcutaneous injection in C57BL/6 mice. AuNP-miRNA release from the PNP hydrogel *in vitro* demonstrates a linear pattern over 5 days up to 20%. AuNP-miR-214 transfection in HEK293 results in 33% decrease of Luciferase reporter activity. In the CAVD model, AuNP-miR-214 are tracked into the cytoplasm of human aortic valve interstitial cells. Lastly, 11 days after subcutaneous injection, AuNP-miR-67 predominantly clears *via* the liver and kidneys, and fluorescence levels are again comparable to control animals. Thus, the PNP-AuNP-miRNA drug delivery platform provides linear release of functional miRNAs *in vitro* and has potential for *in vivo* applications.

Received 30th July 2021,
Accepted 21st October 2021

DOI: 10.1039/d1nr04973a

rsc.li/nanoscale

[a]*Regenerative Medicine Center, University Medical Center Utrecht, Uppsalalaan 8, 3584 CT Utrecht, the Netherlands*
[b]*Department of Cardiology, Experimental Cardiology Laboratory, Circulatory Health Laboratory, University Medical Center Utrecht, Utrecht University, Heidelberglaan 100, 3584 CX Utrecht, the Netherlands*
[c]*Center of Excellence in Cardiovascular Biology, Division of Cardiovascular Medicine, Department of Medicine, Brigham and Woman's Hospital, Harvard Medical School, 77 Avenue Louis Pasteur, Boston 02115, MA, USA*
[d]*David H. Koch Institute for Integrative Cancer Research, Massachusetts Institute of Technology, 500 Main Street, Cambridge 02142, MA, USA*
[e]*Macromolecular Engineering Laboratory, Department of Mechanical and Process Engineering, ETH Zurich, Sonneggstrasse 3, 8092 Zurich, Switzerland*
[f]*NOVA Medical School, Faculdade de Ciências Médicas, Universidade Nova de Lisboa, 1169-056 Lisboa, Portugal*
[g]*Centre for Toxicogenomics and Human Health, Genetics, Oncology and Human Toxicology, NOVA Medical School, Faculdade de Ciências Médicas, Universidade Nova de Lisboa, 1169-056 Lisboa, Portugal*
[h]*Netherlands Heart Institute, Moreelsepark 1, 3511 EP Utrecht, the Netherlands*
[i]*Center for Interdisciplinary Cardiovascular Sciences, Division of Cardiovascular Medicine, Department of Medicine, Brigham and Women's Hospital, Harvard Medical School, 3 Blackfan Circle, Boston 02115, MA, USA.*
E-mail: eaikawa@bwh.harvard.edu
[j]*Department of Chemical Engineering, Massachusetts Institute of Technology, 25 Ames Street, Cambridge 02142, MA, USA. E-mail: r.langer@mit.edu*

†Electronic supplementary information (ESI) available See DOI: 10.1039/d1nr04973a

‡Authors contributed equally to this work.

Introduction

Since their discovery, microRNAs (miRNAs) have become a focus of (bio)medical research. The research community has elucidated the role of miRNAs in the etiology and progression of various diseases, including cardiovascular disease,[1–3] cancer,[4,5] and hepatitis C.[6] The discovery of their central role in several pathological conditions has provided the basis for using miRNAs in the treatment of these diseases. For example, miR-34 has been tested in phase I trials to treat multiple types of cancer (ClinicalTrials.gov: NCT01829971, NCT02862145) and miR-122 has been explored for the treatment of hepatitis C.[6] The latter successfully completed phase II, whereas the former two trials were terminated prematurely due to serious adverse events, including enterocolitis, hypoxia/systemic inflammatory response syndrome, colitis/pneumonitis, hepatic failure, and cytokine release syndrome/respiratory failure that could be attributed to the treatment.[7] The mixed outcomes of these trials highlight the potential of miRNA therapeutics and the present challenge in their successful delivery to the targeted cells and tissues.

Prior to clinical testing and application, there are several hurdles for RNA therapeutics to overcome regarding their

delivery, retention, stability, and degradation. To prevent endosomal degradation, miRNAs were functionalized with fusogenic pH-sensitive peptides that enabled endosomal escape.[8] When miRNAs are injected directly, washout is high and retention is low.[9] Carrier vehicles and modifications have been explored to reduce the washout and improve the delivery of miRNAs. We previously described non-viral vectors to improve delivery, including lipids,[10] microbubbles,[11] polymers,[12] and inorganic materials,[13] as well as modifications to improve both biostability and binding stability.[14] Injectable hydrogels are promising candidates to improve and localize the delivery of therapeutic miRNA molecules while allowing minimally invasive application.

Injectable hydrogels have been designed with natural or synthetic polymers, including ECM,[15] collagen, fibrin, alginate, functionalized poly(ethylene glycol) (PEG), or poly(*N*-isopropylacrylamide) (pNIPAM).[16] Traditionally, hydrogels have been based on covalent cross-linking methods that require initiation by temperature,[17] light,[18] or a change in pH.[19–21] For biomedical applications, including drug delivery, these covalent cross-linking methods can provide an additional hurdle, as the cross-linking reaction is not instantaneous, and drugs can be lost during network formation. Additionally, for some materials it requires an external stimulus or an instrument, such as a UV light source. To simplify the application of hydrogels and avoid the challenges associated with covalent cross-linking, non-covalent cross-linking allows for spontaneous gel formation without an external trigger. In addition, non-covalent hydrogels often exhibit shear-thinning (the ability to flow upon application of stress) and self-healing (reformation of the gel upon relaxation of the external stress) properties. Shear-thinning facilitates injection and minimally invasive delivery, thus improving clinical application.

Injectable hydrogels have been developed using leucine zipper domains,[22] dock-and-lock proteins,[23] and host–guest interactions.[24] A pH cross-linkable hydrogel was developed for miRNA delivery based on non-covalent ureido-pyrimidinone (UPy) cross-linking. Near complete release of miRNA molecules from UPy gels was achieved after two days.[21] This release could be extended by modification of the miRNA molecules with cholesterol groups. We recently developed a class of shear-thinning and self-healing hydrogels based on polymer–nanoparticle (PNP) interactions.[25,26] These properties arise from the reversible, non-covalent interactions between the polymer and the nanoparticles within the gel, employing a hydroxypropylmethylcellulose derivative (HPMC-C_{12}) and core–shell nanoparticles [poly(ethylene glycol)-*block*-poly(lactic acid) (PEG-*b*-PLA) nanoparticles].

This research set out to improve both the biostability and the delivery of miRNA. In order to improve biostability and reduce degradation, the miRNA molecules were attached to gold nanospheres (AuNP) that were functionalized with poly(ethylene-glycol) (PEG).[13,27–29] In addition, influenza hemagglutinin (HA1) peptide was added to stimulate endosomal escape intracellularly by destabilizing the endosomal membrane.

These functionalized AuNP (AuNP-miR) were loaded into a biocompatible, shear-thinning, and self-healing injectable hydrogel, based on the PNP gel platform, to improve minimally invasive, local, and sustained delivery. This research shows (1) linear release of AuNP-miRs from the PNP hydrogel over multiple days, and (2) that AuNP-miRs retain functionality *in vitro.* Additionally, it shows that (3) AuNP-miRs retain functionality by employing an *in vitro* miRNA reporter assay and a complex model system, specifically in a 3D *in vitro* model of human calcific aortic valve disease.[30] Lastly, it shows (4) the biodistribution of AuNP-miRs after subcutaneous injection *in vivo*. Together, this data demonstrates an innovative approach to achieve controlled release of functional miRNA from an injectable, self-healing PNP hydrogel.

Results & discussion

Production of AuNP-miR-loaded PNP hydrogels

To engineer an injectable biomaterial for controlled release of miRNAs, we prepared AuNP-miRNAs within PNP hydrogel formulations. We synthesized the PNP hydrogel components and functionalized the AuNPs with PEG, cel-miR-67 or has-miR-214, and HA1-peptide (Fig. S1†). Cel-miR-67 was used as a negative control as it has minimal sequence identity with murine or human miRNAs and it is not naturally present in human cells; thus, it should not have any biological effect. The HA1 peptide, a fusogenic peptide (influenza hemagglutinin HA1 peptide, N-YPYDVPDYA-C23) was used to increase miRNA uptake by destabilizing the endosomal membrane stimulating endosomal discharge by a pH-responsive machinery.[13] This peptide was functionalized on the surface of the AuNPs *via* carbodiimide chemistry assisted by *N*-hydroxisuccinimide using an EDC/NHS coupling reaction between the carboxylated PEG spacer and the amine terminal group of the peptide. HPMC-C_{12} and PEG-*b*-PLA polymers were synthesized as previously described.[25] PEG-*b*-PLA polymers were formulated into NPs *via* nanoprecipitation and characterized by dynamic light scattering (DLS). PEG-*b*-PLA NPs with a diameter (D_h) of ~88 nm and dispersity ($Đ$) of 0.12 were used to formulate the PNP hydrogel. Based on prior work, NPs of this diameter form gels by enabling polymer bridging over several NPs in contrast to polymer wrapping around single NPs.[31] PNP hydrogels were formulated at 1 wt% HPMC-C_{12} and 10 wt% PEG-*b*-PLA NPs (Fig. 1a).

Linear release of AuNP-miRs from PNP hydrogels

To monitor the release of AuNP-miRs from the PNP hydrogels, non-modified AuNPs and AuNP-miR-67 were loaded into the PNP hydrogel in a 1 : 1 : 1 ratio (PEG-*b*-PLA : HPMC-C_{12} : AuNP; final concentration AuNP-miR-67 0.34 nM) and incubated at 37 °C, 5% CO_2. The supernatant was collected and replaced at 24 h intervals to quantify the concentration of AuNPs in the supernatant based on a calibrated absorbance measurement (Fig. S2†). Sustained linear release of AuNP-miR-67 was observed up to ~20% of the loaded AuNPs over the course of 5

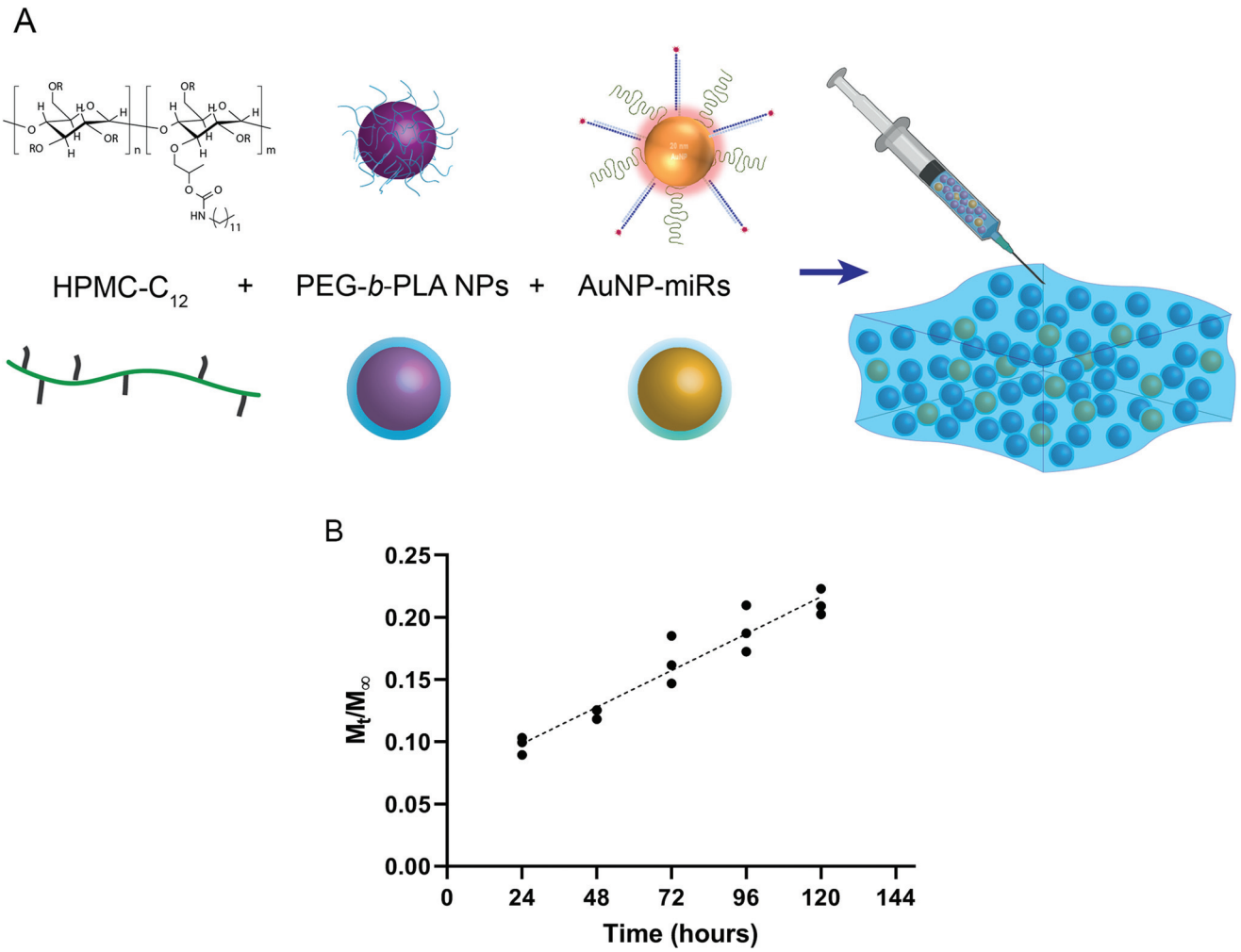

Fig. 1 (A) schematically represents the structure of the PNP hydrogel and the functionalized AuNP-miRs. (B) Depicts *in vitro* release profile of AuNP-miRs from the PNP hydrogel at 37 °C demonstrating the cumulative sustained release of AuNP-miRs in a linear pattern of up to ~20% [M_t/M_∞; the cumulative fractional mass released at time t (n = 3)]. R^2 = 0.9875, M_t/M_∞ = 0.0012 t + 0.0688.

days (Fig. 1b), demonstrating extended release compared to other hydrogel-based drug-delivery systems.[14,20,31–33,35] Following an initial burst release of ~10% of the loaded AuNP over the first 24 h, ~3% of the loaded AuNP were released per day over the course of 5 days. The observed linear release was consistent with an erosion-based release that has been observed for NP release from PNP hydrogels.[25]

AuNP-miR-214 demonstrates *in vitro* mRNA targeting activity

Next, we verified the mRNA targeting capacity of miR-214 after conjugation to the AuNPs. HEK293 cells were transfected with a miR-214 target luciferase reporter[34] and incubated with AuNP-miR-214s. Compared to a non-transfected control and an inactive AuNP-miR-67 control, AuNP-miR-214 significantly reduced the Luciferase signal (~42%) after 48 h, demonstrating preserved miR-214 bioactivity after coupling to the AuNP (Fig. 2). As a positive control, transfection with unmodified miR-214 mimics using Lipofectamine resulted in a knockdown of ~67% relative to the control groups. The higher transfection efficiency of Lipofectamine compared to AuNP-miR-214 is expected, considering the thorough optimization of commercially available Lipofectamine.

Suppression of a target gene up to 90% has been observed for small interfering RNA (siRNA) released from alginate or collagen hydrogels in a green fluorescent protein (GFP) expressing HEK293 cell line,[33] though over a longer time scale of 6 days. 80% knockdown of GFP signal was achieved with miRNA released from a PEG hydrogel over a period of 42 days.[36] This suggests that an extended testing period for AuNP-miR-214 should be considered for translational use.

AuNP-miR-67 infiltrate haVICs in a 3D bioprinted *in vitro* CAVD model

In order to test AuNP-miR uptake in a more complex tissue model, we tracked fluorescently labelled AuNP-miR-67 in a 3D model of CAVD. Cel-miR-67 was used as a negative control as it has minimal sequence identity with murine or human miRNAs and it is not naturally present in human cells; thus, it

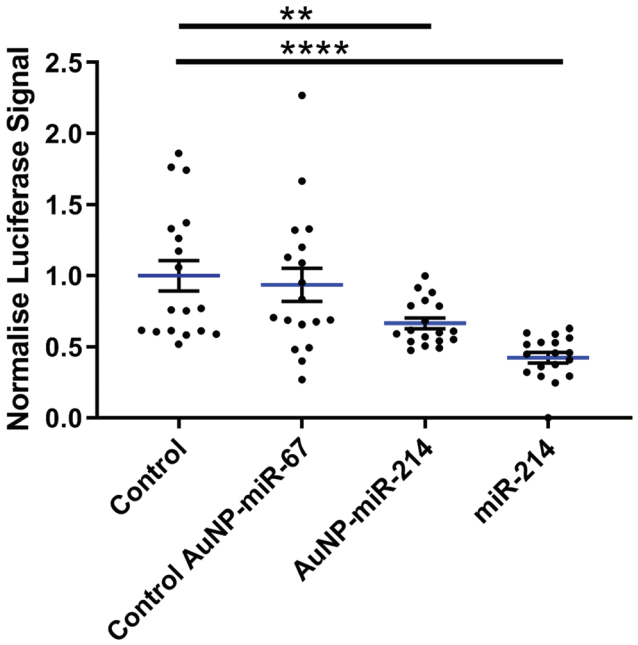

Fig. 2 AuNP-miR-214 significantly reduces Luciferase activity. AuNP-miR-214 were added to HEK293 cells introduced to the pMIR-REPORT-QKI-3′ UTR Luciferase vector *in vitro*. Compared to an untransfected control and an inactive control AuNP-miR-67, AuNP-miR-214 suppresses the Luciferase signal (~42%) after 48 h. Transfection with miR-214 mimic using Lipofectamine results in knockdown of ~67% relative to the control groups, compared to ~42% in the AuNP-miR-214 transfection. Mean ± SEM; * $p < 0.05$, ** $p < 0.01$, *** $p < 0.001$; $n = 6$, experiment conducted in triplicate.

should not have any biological effect. Cy5.5-labelled AuNP-miR-67 were added to the cell culture media of a 3D bioprinted model of CAVD containing human aortic valve interstitial cells (haVICs).[30] In this model, VICs cultured in NM maintain a quiescent phenotype and VICs exposed to OM produce micro-calcifications (Fig. S3†). Labeling nuclei with Hoechst (blue), cytoplasm with CellTracker Green (green), and lysosomes with LysoTracker Red (red) aided in demonstrating that AuNP-miR-67 (white) were taken up by the cells in lysosomes (Fig. 3a), indicated by co-localization (pink arrows) of CellTracker Red and the Cy5.5-labelled AuNP-miR-67 (Fig. 3b). We hypothesize that AuNP-miRs are taken up *via* endocytosis, indicated by co-localization (pink arrows) of CellTracker Red and white AuNP-miR-67, and that they can escape the lysosomes, indicated by the presence of both lysosomes (red arrows) and AuNP-miRs (white arrows).

AuNP-miR-214 increase alkaline phosphatase expression in a 3D CAVD model

Additionally, we employed the 3D bioprinted *in vitro* human CAVD model to test AuNP-miR-214 functionality.[30] Osteogenic medium (OM) has been shown to stimulate the formation of calcium minerals through osteogenic differentiation of haVICs.[30] miR-214 was found to increase calcification of haVICs *in vitro* in traditional 2D cell culture.[37] Here, we demonstrate that compared to non-transfected controls 30 nM AuNP-miR-214 transfection significantly increased ALP activity, a phospholytic enzyme associated with early calcification in CAVD,[38] in haVICs within a 3D-bioprinted *in vitro* model of human CAVD cultured in normal medium (NM) (Fig. 4). Compared to NM, OM increased ALP activity (left column), confirming earlier results.[39] Compared to NM, addition of AuNP-miR-214 significantly increased ALP activity (Fig. 4a top row; Fig. 4b). The difference between the effect of AuNP-miR-214 and OM on haVICs was likely due to the relatively low concentration of AuNP-miR-214 and the prolonged exposure to OM. These findings further support a role for miR-214 in the development of CAVD by stimulating ALP and encourage further investigation.

The involvement of miR-214 in CAVD is a relatively recent discovery, and its precise role in CAVD requires further clarification. miR-214 involvement in CAVD was first identified in porcine AV endothelial cells (paVECs).[40] Specifically, microarray analysis and *ex vivo* validation of healthy ventricular and aortic paVECs RNA yielded differential expression levels of miR-214 as a result of oscillatory shear due to disturbed blood flow. Compared to the ventricularis side, increased expression of miR-214 in the fibrosa side of pAVs resulted in thickening and calcification. Later, in a comparison between valves of healthy controls and patients with calcific aortic stenosis, miR-214 was increased in CAVD patients and osteocalcin, osteopontin, Runx2, and osterix were identified and validated as its targets.[41] Furthermore, in excised AVs from patients with CAVD, increased miR-214 expression was found to play a role in suppressing the apoptosis repressor with caspase recruitment domain ARC.[42] In addition, it was demonstrated that miR-214 stimulates the formation of calcific nodules in haVICs *in vitro via* the MyD88/NF-κB inflammatory pathway.[37] Contradictory to the aforementioned results, in larger microarray studies miR-214 was found low in valves from patients with CAVD compared to non-diseased control valves.[43–45] Furthermore, dynamic stretch on porcine AVs *ex vivo* demonstrated that miR-214 was significantly downregulated during late stage calcification, and addition of miR-214 mimic in static stretch conditions resulted in lower levels of calcification. Therefore, the role of miR-214 in the development of CAVD is complex and needs to be further elucidated.[46]

AuNP biodistribution following subcutaneous implantation in PNP hydrogels

We further investigated the biodistribution of AuNP-miRs following delivery from the PNP hydrogel *in vivo*. In general, parenteral administration of therapeutics or drug delivery systems *via* injection can be achieved easily and in a minimally invasive manner. However, traditional intravenous injections result in relatively short residence time in the body. On the other hand, surgical implantation of a material-based controlled release system provides longer-lasting effects but is more invasive. Injectable hydrogels with controlled release provide an attractive method to administer drugs locally, in a minimally invasive manner, and with extended biological effect. For example, hyaluronic acid-based PNP hydrogels were recently

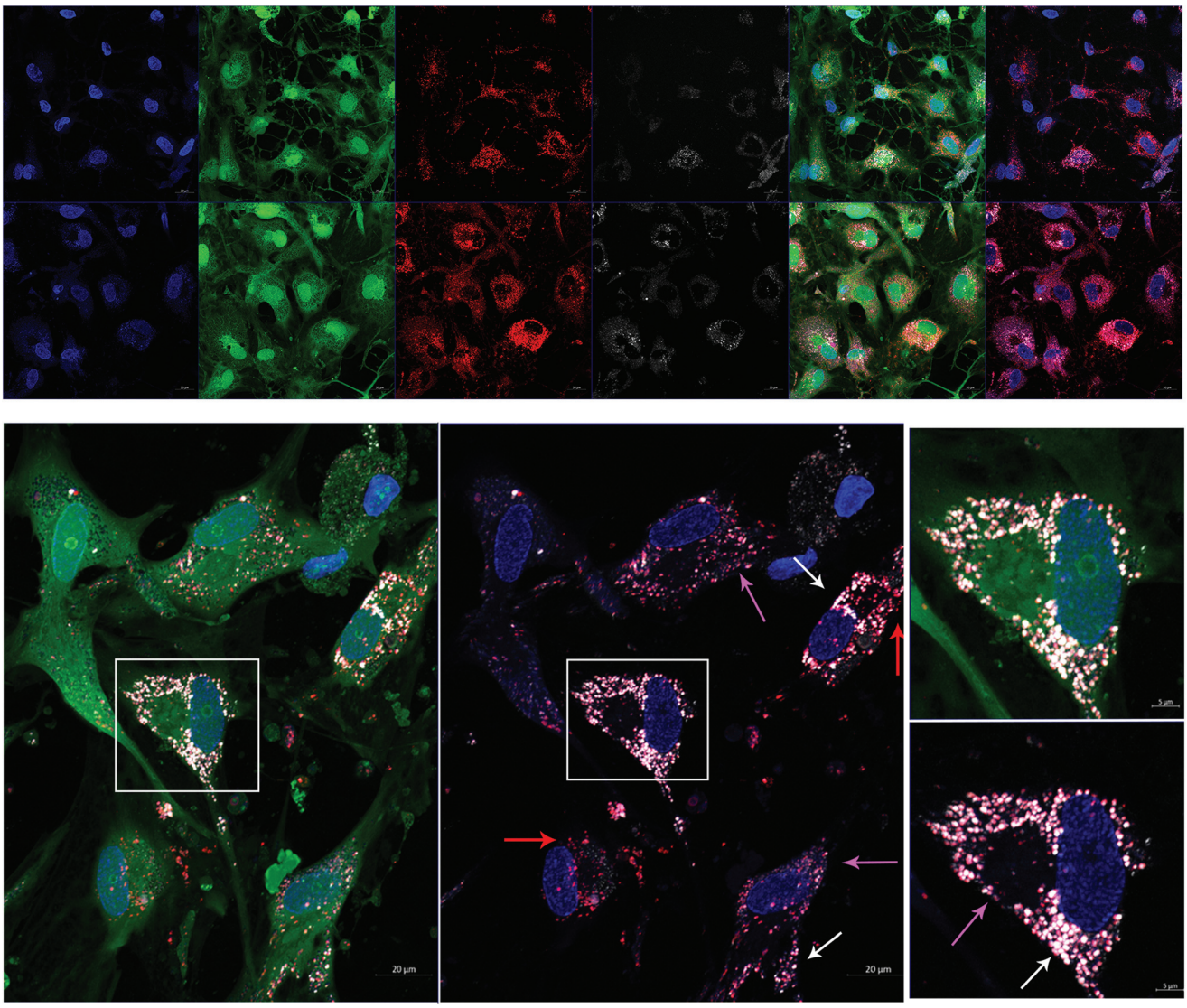

Fig. 3 Infiltration of AuNP-miR-67 into human aortic valve interstitial cells (haVICs) in a 3D bioprinted model of calcific aortic valve disease (CAVD). Nuclei were labelled with Hoechst (blue), haVICs were labelled with CellTracker Green (green), and lysosomes were labelled with LysoTracker Red (red). Co-localization of lysosomes (red) and Cy5.5-labelled AuNP-miR-67 (white) demonstrated that AuNP-miRs were taken up by the cells in lysosomes (scale bar = 20 μm, scale bar insert = 5 μm, t = 48 h, n = 3).

administered to cardiac tissue *via* catheter-based delivery.[47] Therefore, we employed AuNP-miR-loaded PNP hydrogels for administration of an AuNP-miR releasing depot following minimally invasive subcutaneous injection. AuNP-miR-67-loaded PNP hydrogel was injected subcutaneously in nine C57BL/6 mice to assess biodistribution. Cel-miR-67 was used as a negative control as it has minimal sequence identity with murine or human miRNAs and it is not naturally present in human cells; thus, it should not have any biological effect. To monitor the biodistribution of the AuNP-miR, fluorescent signals of the Cy5.5 labelled miR-67 were measured in the lungs, liver, spleen, kidney, and skin surrounding the injection site in three adult male wildtype C57BL/6 mice on days 1, 4, and 11 after injection (Fig. 5). Three additional animals were injected with unloaded PNP hydrogel as negative control and aforementioned tissues were harvested and monitored on day 11. Image quantification of the fluorescent signal of the labelled AuNP-miR-67 demonstrated accumulation in the lungs, spleen, liver and kidney on day 1 and suggests clearance *via* the liver and kidney by day 11, as demonstrated by decreasing fluorescence that approached the values of control animals.

Experimental section

PNP hydrogel synthesis

PNP hydrogels were synthesized as previously described.[25] In short:

HPMC-C12 synthesis. Briefly, hydroxypropylmethylcellulose (HPMC; Sigma h7509-100G; 1.0 g) was dissolved in

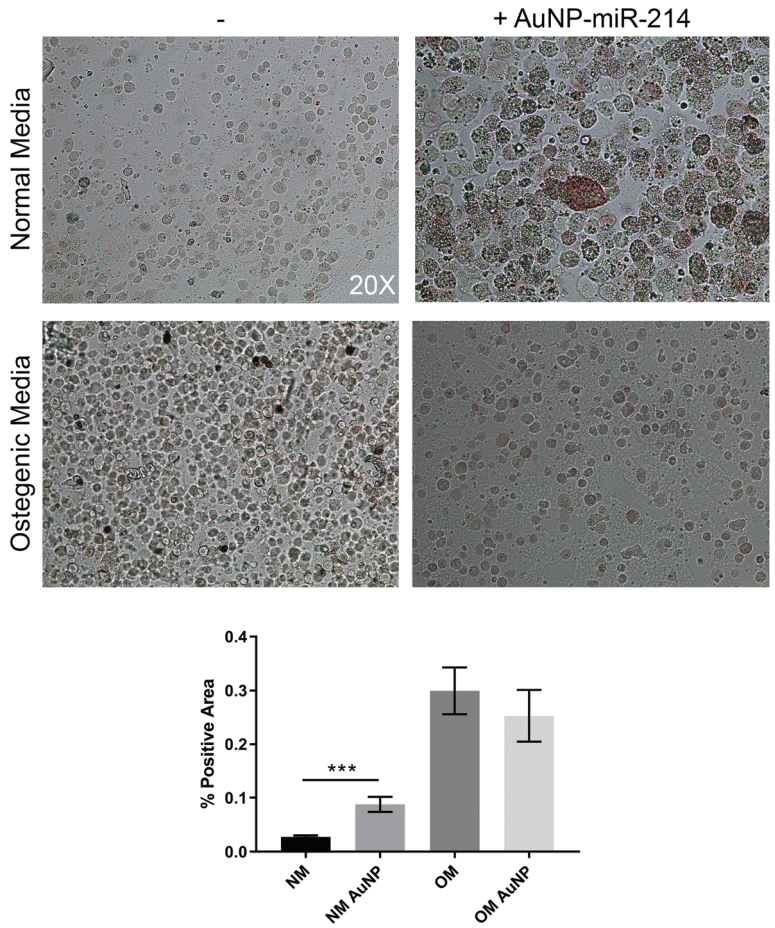

Fig. 4 AuNP-miR-214 increase alkaline phosphatase expression (red) after 48 h in human aortic valve interstitial cells (haVICs) comparable to osteogenic stimulation in 3D human calcific aortic valve disease model. Brightfield microscopy, mean ± SEM, *** $p < 0.001$, $n = 3$, 20× magnification.

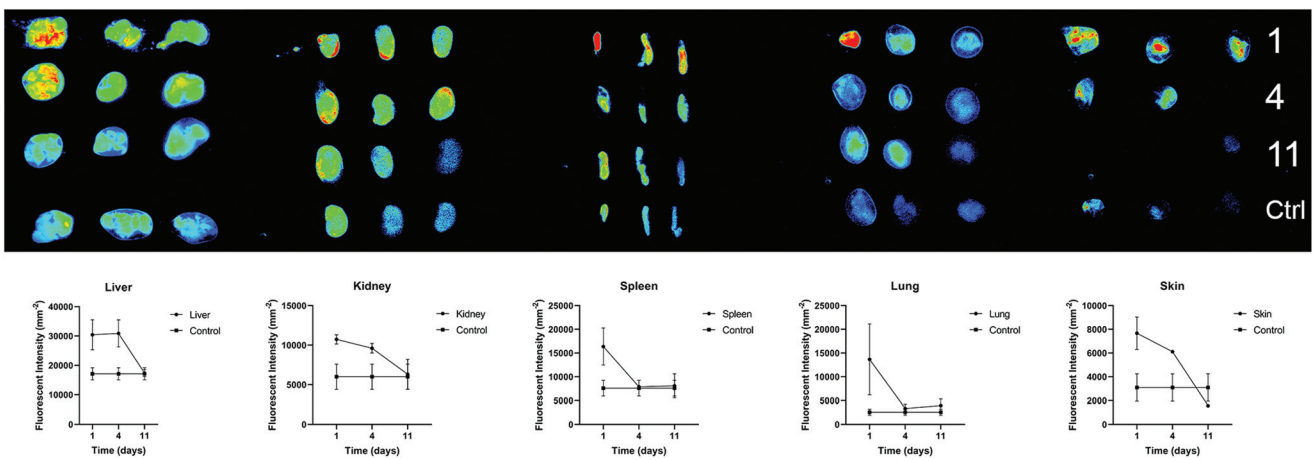

Fig. 5 To assess biodistribution of AuNP-miR-67 $n = 9$ C57BL/6 mice were injected subcutaneously with PNP-AuNP-miR-67. (Top) Fluorescent signals of the Cy5.5 labelled AuNP-miR-67 were measured in the lungs, liver, spleen, kidney, and skin surrounding the injection site in $n = 3$ animals on days 1, 4, and 11 after injection. $N = 3$ mice were injected with unloaded PNP hydrogel as a control and aforementioned tissues were harvested on day 11. Intensity of the fluorescent signal of labelled AuNP-miR-67 demonstrates accumulation in the lungs, spleen, liver and kidney on day 1 and clearance *via* the kidneys after 11 days, as demonstrated by decreasing fluorescent signal comparable to control animals. (Bottom) Quantified fluorescent signal in liver, kidney, lung, spleen, and skin surrounding the injection site on days 1, 4, and 11 demonstrates clearance over 11 days. $N = 3$ animals per time point. Mean ± SEM.

N-methylpyrrolidone (NMP; 45 mL) by magnetic stirring at 80 °C for 1 h. After cooling the solution to room temperature, a solution of 1-dodecylisocyanate (Sigma 389064-5G; 0.5 mmol) and triethylamine (2 drops) were dissolved in *N*-methylpyrrolidone (Sigma PHR1352-2G; 5 mL) and added to the reaction mixture. The mixture was stirred at room temperature for 16 h. This solution was then precipitated from acetone and filtered to recover the polymer, which was dried under vacuum at room temperature for 24 h and weighed, yielding the functionalized HPMC-C_{12} as a white amorphous powder (0.96 g, 87%).

PEG-*block*-PLA synthesis. PEG (Sigma 373001-250G; 0.25 g, 4.1 mmol) and 1,8-diazabicyloundec-7-ene (DBU; Sigma 139009-25G; 10.6 mg, 10 mL, 1.0 mol% relative to LA) were dissolved in dichloromethane (DCM; 1.0 mL). LA (Sigma 767344-5G; 1.0 g, 6.9 mmol) was dissolved in DCM (3.0 mL) with mild heating. The LA solution was then added rapidly to the PEG/DBU solution and stirred rapidly for 10 min. Acetone (7.0 mL) addition then quenched the reaction and the PEG-*b*-PLA copolymer was precipitated from cold diethyl ether, filtered for collection, and lyophilized to yield a white amorphous polymer (1.15 g, 92%). GPC (THF): M_n ($Đ$): 25 kDa (1.09).

PEG-*block*-PLA NP preparation. A solution of PEG-*b*-PLA in DMSO (40 mg mL^{-1}) was added dropwise to water (10 v/v) under a high stir rate. NPs were purified by ultracentrifugation over a filter (molecular weight cut-off of 10 kDa; Millipore Amicon Ultra-15) and resuspended in water to a final concentration of 150 mg mL^{-1}. NP size and dispersity were characterized by DLS.

PNP hydrogel preparation. PNP gels were prepared by first dissolving the HPMC-C_{12} polymer in water (3 wt%, 30 mg mL^{-1}) with stirring and mild heating. NPs were concentrated to 15 wt% solutions. HPMC-C_{12} polymer solution (100 mg) and NP solution (200 mL) were then combined and mixed well by alternately vortex and centrifugation (to remove air bubbles arising from mixing).

AuNP-miR synthesis

AuNP-miRs were synthesized as previously described.[13] In summary:

Functionalization of AuNP with PEG. Briefly, bare AuNP (20 nm gold nanospheres from Cytodiagnostics Inc. G-20–1000; 10 nM) dispersed in aqueous solution of 18 MEG DI Water were mixed with a commercial hetero-functional PEG (α-Mercapto-ω-carboxy PEG solution, HS-C2H4-CONH-PEG-O-C3H6-COOH, MW. 3.5 kDa, Sigma 712515-100MG; 0.006 mg mL^{-1}) in an aqueous solution of SDS (0.08%). Centrifugation (20 000*g*, 30 min, 4 °C) removed excess PEG, which was quantified by the Ellman's Assay. The excess of thiolated chains in the supernatant was quantified by interpolating a calibration curve set by reacting α-Mercapto-ω-carboxy PEG solution (200 μL) in phosphate buffer (100 μL, 0.5 M, pH 7) with 5,5′-dithio-bis(2-nitrobenzoic) acid (DTNB, 7 μL, 5 mg mL^{-1}) in phosphate buffer (0.5 M, pH 7) and measuring the absorbance at 412 nm after 10 min reaction. The linear range for the PEG chain obtained by this method is 0–0.1 mg mL^{-1} (Abs at 412 nm = 8.0353 × [PEG, mg mL^{-1}] + 0.0486). The number of exchanged chains is given by the difference between the amount determined by this assay and the initial amount incubated with the AuNP. There is a point at which the AuNP becomes saturated with a thiolated layer and is not able to take up more thiolated chains – maximum coverage per AuNP, which was 0.03 mg mL^{-1} of PEG for these AuNP. The AuNP were functionalized with 50% PEG layer in order to leave space for binding the thiolated miRNAs and HA1 peptide (Fig. S1†).

Functionalization of AuNP with miRNA molecules. AuNP were functionalised with Cy5.5-labelled miRNA against hsa-miR-214-3p (ACAGCAGGCACAGACAGGCAGU) or cel-miR-67-5p (CGCUCAUUCUGCCGGUUGUUAUG). Briefly, thiolated miRNA (Thermo Scientific Dharmacon) was dissolved in DTT (1 mL, 0.1 M), extracted three times with ethyl acetate, and further purified through a desalting NAP-5 column (Pharmacia Biotech) according to the manufacturer's instructions. The miRNA was only resuspended in DEPC-water and incubated immediately with AuNP previously functionalized with PEG. The purified thiolated miRNAs (10 μM) were incubated with RNase-free solution of the PEG-AuNP (10 nM) containing 0.08% SDS. Subsequently, the salt concentration was increased from 0.05 to 0.3 M NaCl with brief ultrasonication following each addition to increase the coverage of oligonucleotides on the AuNP surface. After functionalization at 4 °C for 16 h, the particles were purified by centrifugation (20 000*g*, 20 min, 4 °C), and re-suspended in DEPC-water. This procedure was repeated 3 times. The number of miRNA per AuNP was determined by quantification of the excess miRNA oligos in the supernatants collected during synthesis *via* the emission spectra of Cy5.5 (excitation/emission, 688 nm/707 nm) dye in a microplate reader (Varioskan Flash Multimode Reader; Thermo Scientific). All nanoparticle samples and standard solutions of the thiolated-miRNAs were kept at the same pH and ionic strength for all measurements. Fluorescence emission was converted to molar concentrations by interpolation from a standard linear calibration curve prepared with known concentrations of miRNA (Fig. S4†).

HA1 peptide functionalization. The HA1 (N-YPYDVPDYA-C) peptide was coupled to the functionalized AuNP using carbodiimide chemistry assisted by *N*-hydroxisuccinimide using an EDC/NHS coupling reaction between the carboxylated PEG spacer and the amine terminal group of the peptide. HA1 peptide, which is used to enhance the miRNA uptake, was functionalized on the AuNP after miRNA functionalization. Briefly, 10 nM of NPs-PEG, 1.98 mg mL^{-1} *N*-hydroxysulfosuccinimide (sulfo-NHS, Sigma) and 500 μg mL^{-1} EDC (1-Ethyl-3-(3-dimethylaminopropyl)carbodiimide, Sigma) were incubated in 10 mM MES (2-(*N*-morpholino)ethanesulfonic acid, Sigma) at pH 6.2 and allowed to react for 30 min to activate the carboxylic groups. After this, activated AuNP were washed once with 10 mM MES, pH 6.2 and used immediately. HA1 was added to the mixture (final concentration 3 μg mL^{-1}) and allowed to react for 16 h at 25 °C. After this period, the AuNP were centrifuged at 20 000*g* for 30 min at 4 °C and washed three times with Milli-Q water.

HA1 quantification was performed with the Pierce® BCA Protein Assay kit (Thermo Scientific) according to manufacturer' instructions. Briefly, each standard (0.025 mL) and unknown sample (the supernatants; 0.025 mL) was mixed with the BCA™ Working Reagent (50 : 1, BCA reagent A : BCA reagent B; 0.2 mL) to each tube. The reaction mixture was incubated at 60 °C for 30 min. After incubation, the tubes were cooled down to room temperature and the absorbance measured at 562 nm. The standard curve was used to determine the HA1 concentration of each unknown sample (supernatant). The calibration curve for a working range (0–125 μg mL^{-1}) is given by the following equation Abs 562 nm = 0.0036 × [HA1 peptide, μg mL^{-1}] + 0.8016, R^2 = 0.9939 for HA1 peptide (Fig. S4†).

Release of AuNP-miRs from PNP hydrogel

AuNP-miR-214 were loaded into PNP hydrogels and incubated at 37 °C, 5% CO_2 with MilliQ water in 1.5 mL Eppendorf tubes. Supernatant was collected at regular 24 h intervals and the absorbance of the supernatant was measured at 524 nm on a Tecan Infinite 200 (Tecan Group Ltd. Männedorf, Switzerland) plate reader from 400 nm to 700 nm. The calibration curve based on a standard series of AuNP and AuNP-miRs (0.0–1.0 nM) is given by the following equations: Abs 524 nm = 0.299 × [AuNP] + 0.0044, R^2 = 0.9984, and Abs 524 nm = 1.4239 × [AuNP-miRs] – 0.0048, R^2 = 0.9986, respectively.

HEK293 cell culture

Human embryonic kidney 293 (HEK293) cells were cultured in Dulbecco's Modified Eagle's Medium (DMEM; ThermoFisher Gibco, supplemented with 10% FBS (ThemoFischer Gibco), 1% Pen/Strep (ThermoFisher Gibco 15070063), 1% Non-Essential Amino Acids NEAA (ThermoFisher Gibco11140050), 1% Sodium Pyruvate (ThermoFisher Gibco, 11360070), on 2% gelatin coated until confluent. For experiments, cells were seeded at 25 000 cells per well in media (100 μL) in a 96 well plate.

Luciferase/beta-galactosidase cell transfection and reporter assay. Cells were transfected at 60–70% confluence with Luciferase and beta-Galactose (β-Gal) pMIR-REPORT vectors as previously described.[34] Briefly, the conserved miR-214-binding sequences in the Quaking (QKI) 3′ untranslated region (UTR) were cloned into the pMIR-REPORT Luciferase vector (Ambion).

To assess the suppression efficiency of AuNP-miR-214, HEK293 cells were co-transfected with pMIR-REPORT-QKI-3′ UTR Luciferase vector (100 ng) and a pMIR-REPORT β-Gal control plasmid (100 ng) in OptiMEM for 4 h to evaluate transfection efficiency. Subsequently, pre-miR-214 (60 nM) was delivered using Lipofectamine 3000 (ThermoFisher, L3000015). AuNP-miR-214 and AuNP-miR-67, as a scramble control microRNA, were added directly to the OptiMEM. Luciferase and β-Gal activity was assessed after 48 h with the Steady-Glo Luciferase Assay Kit (Promega E2520) and β-Gal assay buffer (200 mM sodium phosphate, 2 mM magnesium chloride, 100 mM beta-mercaptoethanol, 1.33 mg mL^{-1} *ortho*-nitrophenyl-β-galactoside (ONPG) in water), respectively. Luciferase activity was assessed by measuring luminescence and β-Gal activity was determined by measuring absorbance at 405 nm and 570 nm. Six biological replicates were transfected per conditions. Experiments were conducted in triplicate.

3D Calcific aortic valve disease (CAVD) model

A 3D *in vitro* model of human CAVD was employed to image AuNP-miRs uptake into cells. We previously published a detailed description and validation of this model.[30] Briefly, human aortic valves were obtained from patients undergoing valve replacement surgery at Brigham and Women's Hospital (Boston, MA, USA) as a result of aortic valve (AV) calcific stenosis. Leaflets were obtained and utilized in accordance with protocols approved by the Institutional Review Board (IRB protocol #2011P001703/PHS). Valvular interstitial cells (VICs) were isolated as previously described.[48] In short, CAVD AV leaflets were cut into 5 mm × 5 mm pieces, incubated in collagenase (Roche 10103586001; 10 mL) solution at 37 °C, 5% CO_2 for 12 h, and homogenized with a serological pipette. The digested tissue was centrifuged, the supernatant aspirated, and the pellet resuspended in VIC cell culture media [DMEM supplemented with 10% FBS (ThermoFisher, Gibco) and 1% P/S (ThermoFisher, Gibco); 5 mL]. The cells were then centrifuged a second time, resuspended in VIC cell culture media (10 mL), and plated in a T75 culture flask. Media was replenished every 48 h. VICs of passage five were used for further experiments. VICs were incorporated in hydrogel pre-polymers by mixing VICs and media (to a final concentration of 10×10^6 cells per mL in the gel) with a GelMA (10 wt%), HAMA (3 wt%), and LAP solution (5 wt%) at 37 °C to form a GelMA (5%), HAMA (1%), and LAP (0.3%) hydrogel. GelMA and HAMA were synthesized as previously described.[49,50]

Constructs were designed in Tinkercad (AutoDesk, Inc., San Rafael, CA, USA), and encoded using Repetier-Host (version 2.0.0; Hot-World GmbH & Co. KG, Willich, Germany), and Sublime Text 3 (Sublime HQ, Pty Ltd., Darlinghurst, NSW, Australia). 3D bioprinting was performed using the Inkredible + (Cellink, Cambridge, MA, USA). Pluronic gel (Pluronic F-127; Allevi, Philadelphia, PA, USA) was printed as a cylindrical mold (outer diameter = 9.0 mm, inner diameter = 8.6 mm, height = 1.5 mm) using a stainless steel needle nozzle (JG27-0.25HPX; Jensen Global Inc., Santa Barbara, CA, USA) at a fill density of 95%, layer height of 0.1 mm, printing speed of 4 mm s^{-1}, and printing pressure of 320 kPa. The second extruder was filled with the required hydrogel pre-polymer compositions and heated to 37 °C. A hydrogel disc was then printed inside the mold from the second extruder using a 23 g stainless steel nozzle (Fisnar 5901005, Ellsworth Adhesives, Germantown, WI, USA) by opening the valve of the second extruder for 40 ms at 15–20 kPa. Cross-linking the pre-polymers for 90 s with 365 nm UV light produced 8.6 mm × 1.0 mm hydrogel discs. The UV light was calibrated to an intensity of 2.5 mW cm^{-2} using a radiometer (85009, Sper Scientific Direct, Scottsdale, AZ, USA). After printing, the Pluronic gel was dissolved by washing in cold PBS. One day after printing, hydro-

gels were switched to normal media (NM; 10% FBS, 1% P/S) or osteogenic media (NM supplemented with 10 nM dexamethasone, 10 ng mL^{-1} ascorbic acid, and 10 mM β-glycerolphosphate) as previously described,[51] for up to 14 days. Media was changed every 48 h for all constructs. Cells were transfected with miR-214 (30 nM) by addition of AuNP-miR-214 to the cell culture media 48 h prior to imaging.

CellTracker/LysoTracker and confocal imaging

To trace the AuNP-miRs into the cells in the 3D CAVD model LysoTracker Red (ThermoFisher, L7528; 50 nM), CellTracker Green (ThermoFisher, C2925; 10 mM) dyes, and Hoechst 33342 (ThermoFisher, H1399) were added according to the manufacturer's protocol. CellTracker Green was incubated overnight at 37 °C, 5% CO_2, LysoTracker Red was incubated for 1 h at 37 °C, 5% CO_2, Hoechst (1 : 5000) was added and incubated for 30 min at 37 °C, 5% CO_2, prior to imaging. Z-stack images of the constructs were taken on a ZEISS LSM 880 Confocal Microscope with AiryScan.

Animal procedures

All animal procedures were performed according to MIT Animal Care and Use Committee approved protocols. Adult male C57BL/6 mice were injected subcutaneously on the back with PNP-AuNP-miR-67 gels (100 μL; HPMC-C_{12} 1 wt%; PEG-*b*-PLA NPs 10 wt%; AuNP-miR-67 85 nM) using a 26G syringe. At 1, 4, and 11 days following injection 3 animals per time point were sacrificed and lung, spleen, liver, kidneys and the tissue surrounding the injection site were harvested, flash-frozen, and stored until further analysis. Fluorescence reflectance of tissues was measured using a Kodak Image Station 4000 mm Pro.

Statistics

Quantitative data is given as mean ± standard error. The number of independent experiments is given as n. Statistical analyses were performed with GraphPad Prism 7 (GraphPad Software, La Jolla, CA, USA), Student's *t*-tests were performed for two-group comparisons, and for multiple group comparisons one-way or two-way ANOVA with Tukey's *post-hoc* HSD tests were used as appropriate. *P*-Values < 0.05 were considered statistically significant.

Conclusion

In conclusion, our data demonstrate that AuNP-miRs can be delivered *via* a minimally invasive, injectable self-assembling hydrogel, expressing controlled release. We showed that approximately 20% of AuNP-miRs were released from the PNP hydrogel over 5 days. Additionally, we observed that AuNP-miR-214 remained functional after delivery in both a 2D *in vitro* miR-214 target luciferase reporter assay and in a 3D bioprinted human CAVD model. Furthermore, we demonstrated that AuNP-miRs were cleared after 11 days in mice following subcutaneous injection of the PNP-AuNP-miR hydrogel delivery system. Without any cell-targeting ligands, these subcutaneously administered AuNP-miRs were taken up by the spleen, lungs, and liver, and were disposed *via* renal excretion. Additional targeting ligands and site- specific delivery could tailor this platform to specific cells or tissues, especially in combination with RNAi molecules adapted to a specific tissue, cell type, or disease.

Author contributions

Conceptualization: CV, MWT, JC, EA. Data curation: – Formal Analysis: CV, MWT, JC. Funding acquisition: CV, PD, JS, EA, RL. Investigation: CV, MWT, JC. Methodology: CV, MWT, JC, AM. Project administration: EA, RL. Resources: AM, JH, JS, EA, RL. Software: – Supervision: AM, JH, JS, EA, RL. Validation: CV, MWT, JC. Visualization: CV, MWT, JC. Writing – original draft: CV, MWT, JC. Writing – review & editing: AM, JH, PD, JS, EA, RL.

Conflicts of interest

J.C. is a co-founder and shareholder of TargTex S.A.

Acknowledgements

This research was funded by the National Institutes of Health (NIH) R01 grants R01HL 141719, R01HL136431 and R01HL147095 (E.A.); the National Institutes of Health grant EB000244 (to R.L.); the Netherlands CardioVascular Research Initiative (CVON: The Dutch Heart Foundation, Dutch Federation of University Medical Centers, the Netherlands Organization for Health Research and Development, and the Royal Netherlands Academy of Science) and Vrienden UMC Utrecht (C.V., J.S.); an unrestricted grant from CELLINK to Vrienden UMC Utrecht (C.V., J.S.); the Harvard Catalyst Advanced Microscopy Pilot grants (C.V., E.A.); and the NIH Ruth L. Kirschstein National Research Service Award F32HL122009 (M.W.T.). J.C. acknowledges the European Research Council Starting Grant (ERC-StG-2019-848325). This work was conducted with support from Harvard Catalyst | The Harvard Clinical and Translational Science Center (National Center for Advancing Translational Sciences, National Institutes of Health Award UL1 TR001102) and financial contributions from Harvard University and its affiliated academic healthcare centers. We thank the Harvard Center for Biological Imaging for infrastructure and support, in particular Dr D. Richardson and S. Terclavers. The authors would like to thank Elia Guzzi for assistance with hydrogel preparation.

References

1 A. Eulalio, M. Mano, M. Dal Ferro, L. Zentilin, G. Sinagra, S. Zacchigna and M. Giacca, *Nature*, 2012, **492**, 376.
2 C. Wahlquist, D. Jeong, A. Rojas-Muñoz, C. Kho, A. Lee, S. Mitsuyama, A. van Mil, W. J. Park, J. P. Sluijter,

P. A. Doevendans, R. F. Hajjar and M. Mercola, *Nature*, 2014, **508**, 531.
3 A. Aguirre, N. Montserrat, S. Zacchigna, E. Nivet, T. Hishida, M. N. Krause, L. Kurian, A. Ocampo, E. Vazquez-Ferrer, C. Rodriguez-Esteban, S. Kumar, J. J. Moresco, J. R. Yates, 3rd, J. M. Campistol, I. Sancho-Martinez, M. Giacca and J. C. Izpisua Belmonte, *Cell Stem Cell*, 2014, **15**, 589.
4 H. Hosseini, M. M. S. Obradović, M. Hoffmann, K. L. Harper, M. S. Sosa, M. Werner-Klein, L. K. Nanduri, C. Werno, C. Ehrl, M. Maneck, N. Patwary, G. Haunschild, M. Gužvić, C. Reimelt, M. Grauvogl, N. Eichner, F. Weber, A. D. Hartkopf, F. A. Taran, S. Y. Brucker, T. Fehm, B. Rack, S. Buchholz, R. Spang, G. Meister, J. A. Aguirre-Ghiso and C. A. Klein, *Nature*, 2016, **540**, 552.
5 J. Su, S. M. Morgani, C. J. David, Q. Wang, E. E. Er, Y. H. Huang, H. Basnet, Y. Zou, W. Shu, R. K. Soni, R. C. Hendrickson, A. K. Hadjantonakis and J. Massagué, *Nature*, 2020, **577**, 566.
6 M. H. van der Ree, J. M. de Vree, F. Stelma, S. Willemse, M. van der Valk, S. Rietdijk, R. Molenkamp, J. Schinkel, A. C. van Nuenen, U. Beuers, S. Hadi, M. Harbers, E. van der Veer, K. Liu, J. Grundy, A. K. Patick, A. Pavlicek, J. Blem, M. Huang, P. Grint, S. Neben, N. W. Gibson, N. A. Kootstra and H. W. Reesink, *Lancet*, 2017, **389**, 709.
7 D. S. Hong, Y. K. Kang, M. Borad, J. Sachdev, S. Ejadi, H. Y. Lim, A. J. Brenner, K. Park, J. L. Lee, T. Y. Kim, S. Shin, C. R. Becerra, G. Falchook, J. Stoudemire, D. Martin, K. Kelnar, H. Peltier, V. Bonato, A. G. Bader, S. Smith, S. Kim, V. O'Neill and M. S. Beg. 2020 Apr 2. Epub ahead of print.
8 S. Oliveira, I. van Rooy, O. Kranenburg, G. Storm and R. M. Schiffelers, *Int. J. Pharm.*, 2007, **331**, 211.
9 A. van Mil, P. A. Doevendans and J. P. Sluijter, *Mini-Rev. Med. Chem.*, 2009, **9**, 235.
10 O. S. Fenton, K. J. Kauffman, J. C. Kaczmarek, R. L. McClellan, S. Jhunjhunwala, M. W. Tibbitt, M. D. Zeng, E. A. Appel, J. R. Dorkin, F. F. Mir, J. H. Yang, M. A. Oberli, M. W. Heartlein, F. DeRosa, R. Langer and D. G. Anderson, *Adv. Mater.*, 2017, **29**(33), DOI: 10.1002/adma.201606944.
11 R. F. Kwekkeboom, J. P. Sluijter, B. J. van Middelaar, C. H. Metz, M. A. Brans, O. Kamp, W. J. Paulus and R. J. Musters, *J. Controlled Release*, 2016, **222**, 18.
12 A. Kargaard, J. P. G. Sluijter and B. Klumperman, *J. Controlled Release*, 2019, **316**, 263.
13 J. Conde, N. Oliva, Y. Zhang and N. Artzi, *Nat. Mater.*, 2016, **15**, 1128.
14 C. F. T. van der Ven, P. J. Wu, M. W. Tibbitt, A. van Mil, J. P. G. Sluijter, R. Langer and E. Aikawa, *Clin. Sci.*, 2017, **131**, 181.
15 M. J. Hernandez, R. Gaetani, V. M. Pieters, N. W. Ng, A. E. Chang, T. R. Martin, E. van Ingen, E. A. Mol, J. P. G. Sluijter and K. L. Christman, *Adv. Ther. (Weinh)*, 2018, **1**(3), 1800032.
16 N. Bayat, Y. Zhang, P. Falabella, R. Menefee, J. J. Whalen 3rd, M. S. Humayun and M. E. Thompson, *Sci. Transl. Med.*, 2017, **9**(419), eaan3879.
17 D. Q. Wu, T. Wang, B. Lu, X. D. Xu, S. X. Cheng, X. J. Jiang, X. Z. Zhang and R. X. Zhuo, *Langmuir*, 2008, **24**, 10306.
18 J. A. Burdick and K. S. Anseth, *Biomaterials*, 2002, **23**, 4315.
19 Y. S. Pek, A. C. A. Wan, A. Shekaran, L. Zhou and J. Y. A. Ying, *Nat. Nanotechnol.*, 2008, **3**, 671.
20 M. M. Bastings, S. Koudstaal, R. E. Kieltyka, Y. Nakano, A. C. Pape, D. A. Feyen, F. J. van Slochteren, P. A. Doevendans, J. P. Sluijter, E. W. Meijer, S. A. Chamuleau and P. Y. Dankers, *Adv. Healthcare Mater.*, 2014, **3**, 70.
21 M. H. Bakker, E. van Rooij and P. Y. W. Dankers, *Chem. – Asian J.*, 2018, **13**, 3501.
22 W. A. Petka, J. L. Harden, K. P. McGrath, D. Wirtz and D. A. Tirrell, *Science*, 1998, **281**, 389.
23 H. D. Lu, M. B. Charati, I. L. Kim and J. A. Burdick, *Biomaterials*, 2012, **33**, 2145.
24 C. B. Rodell, A. Kaminski and J. A. Burdick, *Biomacromolecules*, 2013, **14**, 4125.
25 E. A. Appel, M. W. Tibbitt, M. J. Webber, B. A. Mattix, O. Veiseh and R. Langer, *Nat. Commun.*, 2015, **6**, 6295.
26 O. S. Fenton, M. W. Tibbitt, E. A. Appel, S. Jhunjhunwala, M. J. Webber and R. Langer, *Biomacromolecules*, 2019, **20**, 4430.
27 A. Gilam, J. Conde, D. Weissglas-Volkov, N. Oliva, E. Friedman, N. Artzi and N. Shomron, *Nat. Commun.*, 2016, **7**, 12868.
28 J. Conde, N. Oliva and N. Artzi, *Proc. Natl. Acad. Sci. U.S.A.*, 2015, **112**, E1278–E1287.
29 J. Conde, A. Ambrosone, V. Sanz, Y. Hernández, V. Marchesano, F. Tian, H. Child, C. C. Berry, M. R. Ibarra, P. V. Baptista, C. Tortiglione and J. M. de la Fuente, *ACS Nano*, 2012, **6**, 8316–8324.
30 D. C. van der Valk, C. F. T. van der Ven, M. C. Blaser, J. M. Grolman, P. J. Wu, O. S. Fenton, L. H. Lee, M. W. Tibbitt, J. L. Andresen, J. R. Wen, A. H. Ha, F. Buffolo, A. van Mil, C. V. C. Bouten, S. C. Body, D. J. Mooney, J. P. G. Sluijter, M. Aikawa, J. Hjortnaes, R. Langer and E. Aikawa, *Nanomaterials*, 2018, **8**, 296.
31 E. A. Appel, M. W. Tibbitt, J. M. Greer, O. S. Fenton, K. Kreuels, D. G. Anderson and R. Langer, *ACS Macro Lett.*, 2015, **4**, 848.
32 E. A. Mol, Z. Lei, M. T. Roefs, M. H. Bakker, M. J. Goumans, P. A. Doevendans, P. Y. W. Dankers, P. Vader and J. P. G. Sluijter, *Adv. Healthcare Mater.*, 2019, **8**(20), e1900847.
33 M. D. Krebs, O. Jeon and E. Alsberg, *J. Am. Chem. Soc.*, 2009, **131**, 9204.
34 A. Van Mil, S. Grundmann, M. J. Goumans, Z. Lei, M. I. Oerlemans, S. Jaksani, P. A. Doevendans and J. P. Sluijter, *Cardiovasc. Res.*, 2012, **93**, 655.
35 N. Segovia, M. Pont, N. Oliva, V. Ramos, S. Borrós and N. Artzi, *Adv. Healthcare Mater.*, 2015, **4**, 271.

36 M. K. Nguyen, O. Jeon, M. D. Krebs, D. Schapira and E. Alsberg, *Biomaterials*, 2014, **35**, 6278.
37 D. Zheng, Y. Zang, H. Xu, Y. Wang, X. Cao, T. Wang, M. Pan, J. Shi and X. Li, *Clin. Res. Cardiol.*, 2019, **108**, 691.
38 E. Aikawa, M. Nahrendorf, D. Sosnovik, V. M. Lok, F. A. Jaffer, M. Aikawa and R. Weissleder, *Circulation*, 2007, **115**, 377.
39 J. Hjortnaes, C. Goettsch, J. D. Hutcheson, G. Camci-Unal, L. Lax, K. Scherer, S. Body, F. J. Schoen, J. Kluin, A. Khademhosseini and E. Aikawa, *J. Mol. Cell Cardiol.*, 2016, **94**, 13.
40 S. Rathan, C. J. Ankeny, S. Arjunon, Z. Ferdous, S. Kumar, J. Fernandez Esmerats, J. M. Heath, R. M. Nerem, A. P. Yoganathan and H. Jo, *Sci. Rep.*, 2016, **6**, 25397.
41 H. X. Xu, Y. Wang, D. D. Zheng, T. Wang, M. Pan, J. H. Shi, J. H. Zhu and X. F. Li, *Clin. Lab.*, 2017, **63**, 1163.
42 M. I. Jan, R. A. Khan, T. Ali, M. Bilal, L. Bo, A. Sajid, A. Malik, N. Urehman, N. Waseem, J. Nawab, M. Ali, A. Majeed, H. Ahmad, S. Aslam, S. Hamera, A. Sultan, M. Anees, Q. Javed and I. Murtaza, *Arch. Biochem. Biophys.*, 2017, **633**, 50.
43 S. Coffey, M. J. Williams, L. V. Phillips, I. F. Galvin, R. W. Bunton and G. T. Jones, *Sci. Rep.*, 2016, **6**, 36904.
44 R. Song, D. A. Fullerton, L. Ao, K. S. Zhao, T. B. Reece, J. C. Jr. Cleveland and X. Meng, *J. Am. Heart Assoc.*, 2017, **6**, e005364.
45 H. Wang, J. Shi, B. Li, Q. Zhou, X. Kong and Y. Bei, *BioMed Res. Int.*, 2017, **2017**, 4820275.
46 E. Aikawa and P. A. Libby, *Circulation*, 2017, **135**, 1951.
47 A. N. Steele, L. M. Stapleton, J. M. Farry, H. J. Lucian, M. J. Paulsen, A. Eskandari, C. E. Hironaka, A. D. Thakore, H. Wang, A. C. Yu, D. Chan, E. A. Appel and Y. J. Woo, *Adv. Healthcare Mater.*, 2019, **8**(5), e1801147.
48 R. A. Gould and J. T. Butcher, *J. Visualized Exp.*, 2010, (46), 2158.
49 J. W. Nichol, S. T. Koshy, H. Bae, C. M. Hwang, S. Yamanlar and A. Khademhosseini, *Biomaterials*, 2010, **31**, 5536.
50 J. A. Burdick, C. Chung, X. Jia, M. A. Randolph and R. Langer, *Biomacromolecules*, 2005, **6**, 386.
51 J. D. Hutcheson, C. Goettsch, S. Bertazzo, N. Maldonado, J. L. Ruiz, W. Goh, K. Yabusaki, T. Faits, C. Bouten and G. Franck, *Nat. Mater.*, 2016, **15**, 335.